Viscous Dissipation and Joule Heating Effects on 3D Magnetohydrodynamics Flow of Williamson Nanofluid in a Porous Medium Over a Stretching Surface With Melting Condition

Nainaru Tarakaramu[1]
Department of Mathematics,
Humanities and Basic Sciences,
Annamacharya Institute of
Technology & Sciences,
Tirupati 517520, Andhra Pradesh, India
e-mail: nainaru.tarakaramu2016
@vitstudent.ac.in

Narsu Sivakumar
Department of Mathematics,
SRM Institute of Science and Technology,
Kattankuluthur 603203, Tamil Nadu, India
e-mail: narsusic@srmist.edu.in

P. V. Satya Narayana
Department of Mathematics, SAS,
Vellore Institute of Technology,
Vellore 632014, Tamil Nadu, India
e-mail: pvsatya@vit.ac.in

Ramalingam Sivajothi
Department of Management,
R L Institute of Management Studies (A Unit of
Subbalakshmi Lakshmipathy College of Science),
Madurai 625022, Tamil Nadu, India
e-mail: sivajothi@slcs.edu.in

The aim of the current article is to demonstrate heat transfer characteristics of Williamson nanofluid flow through a stretching surface with a porous medium in two lateral directions. Heat generation, nonlinear thermal radiation, viscous dissipation, Joule heating, and chemical reaction are also considered in time-independent boundary layer equations of heat and concentration. One more significant boundary condition is the melting condition which is introduced in this study for the purpose of more heat generation and suitable transformations by the satisfied continuity equation are selected, These are used to translate the coupled time-independent partial differential equations into a coupled nonlinear system of ordinary differential equations. The translated equations are computed as numerical solutions by utilizing the Runge–Kutta–Fehlberg (R–K–F) fourth-order algorithm with the help of a shooting procedure in MATLAB (bvp4) programming. The significance of physical emerging nondimensional parameters is predicted through graphs and discussed numerically in detail on mass of conservation, temperature, and concentration. The numerical values of the coefficient of the skin friction are displayed through a table with large enhanced values of nondimensional parameters and heat transfer rate explained in detail through graphs. [DOI: 10.1115/1.4055183]

Keywords: fluid flow, heat and mass transfer, MHD, nanofluids, numerical analysis, thermal radiation

Introduction

Nowadays, most of the research (in fluid dynamic) have been interested or attracted by the heat transfer on non-Newtonian fluid flow through a linear stretching surface with a porous medium, because of outstanding different applications in mechanical engineering (like the flow of plasma, the flow of mercury amalgams and lubrications with heavy oils and greases), scientific fields (food mixing and chime movement in the intestine, groves of fruit trees and crops damage via freezing, and manufacturing of ceramics), industrial processes (hydrometallurgical industry, annealing, fiber technology, drawing, extrusion of a polymer sheet from a dye or electronic chips), and manufacturing processes (manufacturing of ceramics, paper production, cooling of elastic sheets, tinning of copper wire) see Refs. [1,2]. Based on these applications, many scientists are focused on non-Newtonian fluid flow and heat exchange. Non-Newtonian fluids is property of viscosity fluid groups such as anisotropic fluids, polar fluids, and viscoelastic fluids. Of these fluids, Williamson fluid is a viscoelastic fluid. It has been tested experimentally [1,3]. Bilal et al. [2] found to be decreasing in both x- and y-directions for large values of both nonlinearity parameter and Williamson parameter. Malik et al. [4] explored the three-dimensional (3D) flow of pseudoplastic fluid over a linearly stretching surface. The Williamson viscoelastic model was employed by Amanulla et al. [5]. It is a representative of certain industrial polymers. It is solved using the second-order accurate implicit Keller box finite difference method. Moatimid and Hassan [6] analyzed the Routh–Hurwitz theory for dispersion relation. The linear stability of the viscoelastic nanofluid is described through Walter's model. Khan et al. [7] described the effect of thermal radiation on nanofluid Williamson nanofluid flow via unsteady stretching surface. This work has been developed through the homotopy analysis method (HAM). In this study, special attention has been given to the variable fluid property effects on the flow of Williamson nanofluid. Parmar [8] discussed the unsteady convective boundary layer flow of magnetohydrodynamic (MHD) Williamson fluid over an inclined porous stretching sheet, which is analyzed numerically by using the Runge–Kutta–Fehlberg (R–K–F) fourth- and fifth-order algorithm through the shooting approach. They concluded that there are increases of λ (Williamson fluid parameter) and K_p (porosity parameter) for the skin-friction coefficient, whereas the opposite behavior is noted on heat and mass transfer. Bhatti and Rashidi [9] discussed the combined effects of thermo-diffusion and thermal radiation on Williamson nanofluid over a porous stretching sheet. It is solved numerically using the successive linearization method (SLM) and the Chebyshev spectral collocation method (CSCM). Hayat et al. [10] examined the stagnation point flow of Williamson nanoliquid toward a nonlinear stretching sheet. This problem is analytically solved via a homotopic procedure. Recently, some of researchers [11–16] presented a different non-Newtonian nanofluid flow over a stretching surface using the R–K–F fourth-order algorithm through a shooting procedure with the help of MATLAM software.

The melting effect is defined as the temperature at which solid changes to liquid at a particular atmospheric pressure. The melting heat exchanger phenomenon has received demanding

[1]Corresponding author.

Manuscript received December 27, 2021; final manuscript received July 24, 2022; published online August 22, 2022. Assoc. Editor: Chun Yang.

experimental and theoretical studies by upcoming scientists because it has very attractive applications (like glass industry, purification of materials, castings of metals, crystal growth, material processing, latent heat storage, artificial freezing of ground for mining and construction purposes, melting of soil, magma solidification, freezing of soil around the heat exchanger coils of a ground-based pump, melting of permafrost, thawing of frozen grounds, preparation of semiconductor-material thermal energy storage). Recently, Venkateswarlu et al. [17] found that the melting parameter increases for the skin-friction coefficient while opposite behavior was noted on Nusselt number at the solid interface. Hajabdollahi et al. [18] reported that melting heat transfer occurs through relative motion between heating source and a phase change material (PCM). The microstructure of the selective laser melting (SLM) built China low activation martensitic (CLAM) steel plates was analyzed by Huang et al. [19]. Hayat et al. [20] described heat transfer characteristics through the melting process, viscous dissipation, and internal heat generation. The melting performance in different eccentricity (e) and wall temperature (T_w) is obtained through numerical simulation and experiment research was examined by Cao et al. [21]. The melting heat transfer was examined [22–26] with experimental and numerical results.

The term "chemical reaction" is an interaction between two or more chemical reacting species in the presence of catalyst. There are two types of chemical reactions, namely, homogeneous and heterogeneous reactions. If the catalyst and reactions have the same phase then the reaction is called as a "homogeneous reaction" and when reactions and catalyst are in a different phase then it is called a "heterogeneous reaction." These reactions have more applications in industrial processes (like energy transfer in cooling tower, food processing, chemical industries, power and cooling industries for drying, energy transfer in a wet cooling tower, groves of fruit trees, drying evaporation at the surface of a water body, generating electric power, flow in a desert cooler, crops damage because of freezing, chemical vapor deposition on surfaces). The numerical results of homogeneous–heterogeneous reactions on two-dimensional (2D) MHD stagnation point flow over a linear stretching surface were discussed by Ramzan et al. [27]. Krishnamurthy et al. [28] analyzed the impact of chemical reaction on melting heat transfer flow of Williamson nanofluid flow. Ramzan et al. [29] studied the numerical calculation of the coefficient of skin-friction, and local Nusselt and Sherwood numbers are discussed in detail and presented through graphs. Hayat et al. [30] presented the analysis of porous medium and homogeneous–heterogeneous reactions. These results are compared and examined by two cases such as mutliwalled carbon nanotubes (MWCNTs) and single-walled carbon nanotubes (SWCNTs). Some authors [31–34] studied heat and mass transfer with chemical reaction influence on magnetohydrodynamic flow in a porous medium over a stretching surface. Recently, some researchers [35–37] studied non-Newtonian fluid with a chemical reaction.

The radiative heat transfer has a more significant influence due to tremendous applications such as power generation and nuclear reactor cooling. The nonlinear thermal radiation effect on 3D Jeffrey nanofluid was explored by Ganesh Kumar et al. [38]. Some authors [39–41] explored the nonlinear thermal radiation effect on non-Newtonian fluid with convective heat transfer. Hayat et al. [42] analyzed how the convergence series solutions are solved by the homotopic procedure. López et al. [43] determined the optimum values of slip flow with minimum values of global entropy generation rate and also calculated Nusselt number and explored for different conditions.

The major importance of this article is heat generation on MHD Williamson nanofluid flow over a linear stretching surface with Joule heating and viscous dissipation, and nonlinear thermal radiation and chemical reaction are presented. The self-similarity variables work to translate time-independent partial differential equations into a system of ordinary differential equations. The transformed equations are solved numerically through a shooting technique in combination with the R–K–F algorithm in MATLAB (bvp4) programming. The impact of physical parameters on interested quantities is discussed in detail by plotting graphs in Fig. 1 and numerical values are mentioned in Table 1.

Mathematical Statement

The 3D MHD Williamson nanofluid flow in a porous medium over a linear stretching surface with viscous dissipation, heat generation, and melting effects is assumed in the stretching flow direction along the x y-surface and the flow is induced by a stretching at $z = 0$. The magnetic field B_0 is applied along the fluid flow direction z. The stretching velocities are taken along the x-direction as $U_w = ax$ and the y-direction as $V_w = by$.

The general equations of the Williamson fluid are given as

$$\nabla \cdot V = 0 \tag{1}$$

$$\rho \frac{dV}{dt} = \nabla \cdot S + \rho b^* \tag{2}$$

The Williamson fluid model equations are given by [1,16,20,41]

$$S = -pI + \tau \tag{3}$$

$$\tau = [(\mu_0 - \mu_\infty)(1 - \Gamma\dot{\gamma})^{-1}]A_1 \tag{4}$$

The first Rivlin–Erickson tensor A_1 and shear rate $\dot{\gamma}$ are defined as

$$\left.\begin{aligned} A_1 = (\nabla \times V) + (\nabla \times V)', \quad \dot{\gamma} = \sqrt{\frac{1}{2}\sum_i \sum_j \dot{\gamma}_{ij}\dot{\gamma}_{ij}\pi} = \sqrt{\frac{1}{2}\pi} \\ \pi = \mathrm{tr}(A_1^2) \end{aligned}\right\} \tag{5}$$

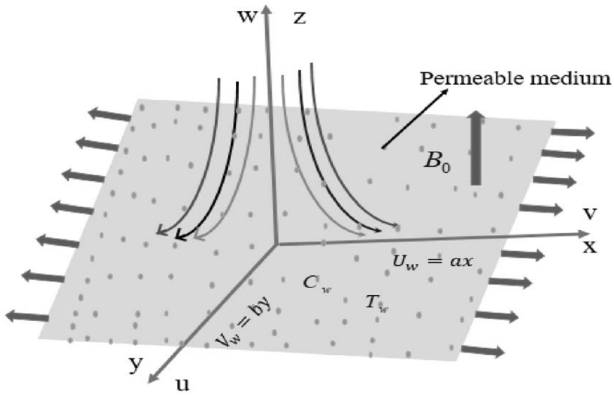

Fig. 1 Physical model of the problem [14,44]

Table 1 Numerical values of $-\mathrm{Re}_x^{1/2}C_{fx}$ and $-\mathrm{Re}_x^{1/2}C_{fy}$ with different parameters of K_p, M for $A = 0$

K_p	M	$-\mathrm{Re}_x^{1/2}C_{fx}$	$-\mathrm{Re}_x^{1/2}C_{fy}$
2.0		1.254	1.254
4.0		1.448	1.443
6.0		1.643	1.638
8.0		1.842	1.83
	2.0	0.001616	0.002293
	4.0	0.00166	0.00251
	6.0	0.002046	0.003081
	8.0	0.002436	0.003689

$$\dot{\gamma} = \left[\left(\frac{\partial u}{\partial x}\right)^2 + \frac{1}{2}\left(\frac{\partial u}{\partial y} + \frac{\partial v}{\partial x}\right)^2 + \left(\frac{\partial v}{\partial y}\right)^2 \right]^{1/2} \tag{6}$$

Consider $\mu_\infty = 0$ and $\Gamma\dot{\gamma} < 1$ thus Eq. (4) can be expressed as

$$\tau = [\mu_0(1 - \Gamma\dot{\gamma})^{-1}]A_1 \tag{7}$$

The extra stress tensor components are

$$\left.\begin{aligned} \tau_{xx} &= 2\mu_0[1 + \Gamma\dot{\gamma}]\left(\frac{\partial u}{\partial x}\right), \quad \tau_{xy} = \tau_{xy} = \mu_0[1 + \Gamma\dot{\gamma}]\left(\frac{\partial u}{\partial y} + \frac{\partial u}{\partial x}\right) \\ \tau_{yy} &= 2\mu_0[1 + \Gamma\dot{\gamma}]\left(\frac{\partial u}{\partial y}\right), \quad \tau_{xz} = \tau_{yz} = \tau_{zx} = \tau_{zy} = \tau_{zz} = 0 \end{aligned}\right\} \tag{8}$$

Considering the above, the governing equations of conservative of mass, conservative of momentum, conservative of energy and concentration are formed as

$$\frac{\partial u}{\partial x} + \frac{\partial v}{\partial y} + \frac{\partial w}{\partial z} = 0 \tag{9}$$

$$u\frac{\partial u}{\partial x} + v\frac{\partial v}{\partial y} + w\frac{\partial w}{\partial z} = \upsilon\frac{\partial^2 u}{\partial z^2} + \sqrt{2\upsilon}\Gamma\frac{\partial u}{\partial z}\frac{\partial^2 u}{\partial z^2} - \frac{\sigma B_0^2}{\rho}u - \frac{\upsilon}{k_p^*}u \tag{10}$$

$$u\frac{\partial u}{\partial x} + v\frac{\partial v}{\partial y} + w\frac{\partial w}{\partial z} = \upsilon\frac{\partial^2 v}{\partial z^2} + \sqrt{2\upsilon}\Gamma\frac{\partial v}{\partial z}\frac{\partial^2 v}{\partial z^2} - \frac{\sigma B_0^2}{\rho}v - \frac{\upsilon}{k_p^*}v \tag{11}$$

$$\left.\begin{aligned} u\frac{\partial T}{\partial x} + v\frac{\partial T}{\partial y} + w\frac{\partial T}{\partial z} &= \alpha_m\frac{\partial^2 T}{\partial z^2} - \frac{1}{(\rho c)_f}\frac{\partial q_r}{\partial z} \\ &+ \zeta\left(D_B\left(\frac{\partial C}{\partial z}\frac{\partial T}{\partial z}\right) + \frac{D_T}{T_\infty}\left(\frac{\partial T}{\partial z}\right)^2\right) \\ &+ \frac{Q_0(T - T_\infty)}{(\rho c_p)} + \frac{\sigma B_0^2}{(\rho c_p)}(u^2 + v^2) \\ &+ \frac{\mu_0}{(\rho c_p)}(u'^2 + v'^2) \end{aligned}\right\} \tag{12}$$

$$u\frac{\partial C}{\partial x} + v\frac{\partial C}{\partial y} + w\frac{\partial C}{\partial z} = D_B\frac{\partial^2 C}{\partial z^2} + \frac{D_T}{T_\infty}\left(\frac{\partial^2 T}{\partial z^2}\right) - K_m(C - C_\infty) \tag{13}$$

The boundary conditions of the present model are

$$\left.\begin{aligned} &u = U_w(x) = ax, \quad v = V_w(x) = by, \quad w = 0, \\ &T = T_w, \quad C = C_w \quad \text{at} \quad z \to 0 \quad u \to 0 \quad v \to 0, \\ &T \to T_\infty, \quad C \to C_\infty \quad \text{as} \quad z \to \infty \end{aligned}\right\} \tag{14}$$

and

$$k\left(\frac{\partial T}{\partial z}\right)_{z=0} = \rho(\beta + c_s(T_m - T_s))w(x, 0, 0) \tag{15}$$

The radiative heat flux q_r which is given by Quinn Brewster [39] is given by

$$q_r = -\frac{4\sigma^*}{3k^*}\frac{\partial T^4}{\partial z} \tag{16}$$

Neglected higher-order terms we get

$$T^4 = 4TT_\infty^3 - T_\infty^4 \tag{17}$$

Differentiating the above heat flux equation, we get

$$\frac{\partial q_r}{\partial z} = -\frac{16\sigma^* T^3}{3k^*}\frac{\partial T}{\partial z} \tag{18}$$

Substituting Eq. (18) in Eq. (12), we get the below expression

$$\left.\begin{aligned} u\frac{\partial T}{\partial x} + v\frac{\partial T}{\partial y} + w\frac{\partial T}{\partial z} &= \alpha_m\frac{\partial^2 T}{\partial z^2} + \frac{1}{(\rho c)_f}\left(\frac{16\sigma^*}{3K^*}\frac{\partial}{\partial z}\left(T^3\frac{\partial T}{\partial z}\right)\right) \\ &+ \zeta\left(D_B\left(\frac{\partial C}{\partial z}\frac{\partial T}{\partial z}\right) + \frac{D_T}{T_\infty}\left(\frac{\partial T}{\partial z}\right)^2\right) \\ &+ \frac{Q_0(T - T_\infty)}{(\rho c_p)} + \frac{\sigma B_0^2}{(\rho c)}(u^2 + v^2) \\ &+ \frac{\mu_0}{(\rho c)}(u'^2 + v'^2) \end{aligned}\right\} \tag{19}$$

The similarity transformations as

$$\left.\begin{aligned} \eta = \sqrt{\frac{a}{\upsilon}}z, \quad u = axf'(\eta), \quad v = ayg'(\eta), \quad w = -\sqrt{a\upsilon}(f(\eta) + g(\eta)) \\ \theta(\eta) = \frac{T - T_\infty}{T_f - T_\infty}, \quad \phi(\eta) = \frac{C - C_\infty}{C_f - C_\infty} \end{aligned}\right\} \tag{20}$$

Solving Eq. (15) by using Eq. (20), we have

$$\left.\begin{aligned} k(T_f - T_\infty)\theta'\sqrt{\frac{a}{\upsilon}} &= \rho(\beta + c_s(T_m - T_s))(-\sqrt{a\upsilon}f) \\ \frac{(T_f - T_\infty)}{(\beta + c_s(T_m - T_s))}\theta' &= -\frac{\rho}{k}\upsilon f \end{aligned}\right\} \tag{21}$$

Using Eq. (19), we are converting Eqs. (9)–(11), (13), and (19) into the below format

$$f'''(1 + \lambda f'') - (f')^2 + f''(f + g) - (M + K_p)f' = 0 \tag{22}$$

$$g'''(1 + \lambda g'') - (g')^2 + g''(f + g) - (M + K_p)f' = 0 \tag{23}$$

$$\left.\begin{aligned} &\Pr((f + g)\theta' - f'\theta + N_b\theta'\phi' + N_t(\theta')^2) \\ &+ ((1 + R_d(1 + (\theta_w - 1)\theta))^3\theta')' + H\theta \\ &+ (Ec_x(f'')^2 + Ec_y(g'')^2) + M^2(Ec_x(f')^2 + Ec_y(g')^2) = 0 \end{aligned}\right\} \tag{24}$$

$$\phi'' + \Pr \mathrm{Le}(f + g)\phi' - (N_t/N_b)\theta'' - K\phi = 0 \tag{25}$$

Corresponding boundary conditions as

$$\left.\begin{aligned} f' = 1, \quad g = 0, \quad g' = A, \quad \theta(0) = 1, \quad \phi'(0) = 0 \quad \text{at} \quad \eta \to 0 \\ f' \to 0, \quad g' \to 0, \quad \theta \to 0, \quad \phi \to 0 \quad \text{as} \quad \eta \to \infty \end{aligned}\right\} \tag{26}$$

and from Eq. (21), we have the melting effect as

$$\Pr f + Mt\theta' = 0 \tag{27}$$

The skin-friction coefficient and local Nusselt number are

$$\mathrm{Re}_x^{1/2}C_{fx} = -f''(0), \quad \mathrm{Re}_x^{1/2}C_{fy} = -g''(0), \quad \mathrm{Re}_x^{-1/2}\mathrm{Nu}_x = -\theta'(0)\} \tag{28}$$

Results and Discussion

The transformed Equations (22)–(25) with boundary conditions (26) and (27) have been solved numerically by the R–K–F fourth-order algorithm along with a shooting procedure. To develop the outstanding results of velocity ($f'(\eta)$, $g'(\eta)$) flows along axial and transverse directions, the heat transfer ($\mathrm{Re}_x^{-1/2}\mathrm{Nu}_x$) rate due to related physical parameters involved in this investigation with numerical solutions is described through their plotted graphs: Figs. 2–8 and displays tabulate values of skin-friction coefficients in x, y-directions. Throughout the study different Williamson

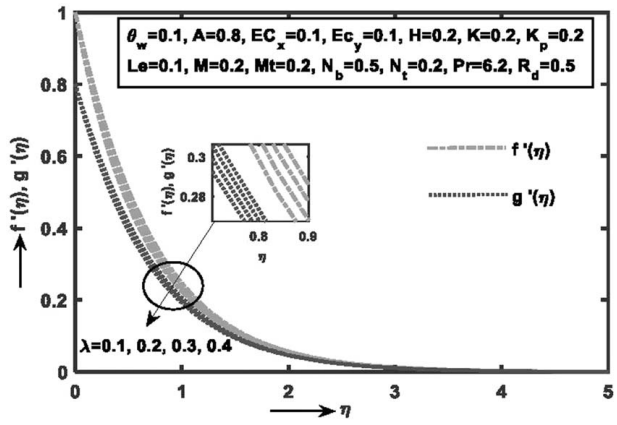

Fig. 2 Impact of λ on $f'(\eta)$, $g'(\eta)$

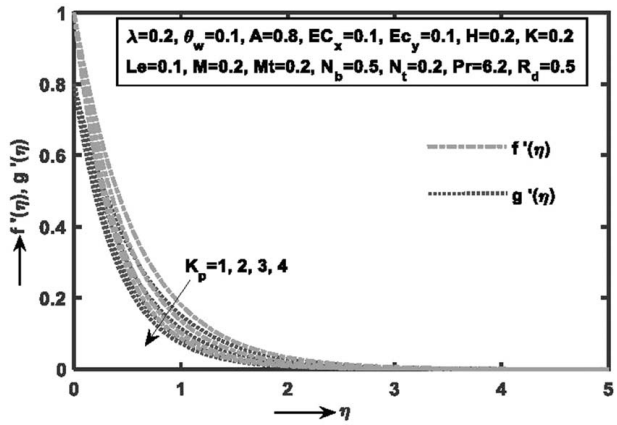

Fig. 3 Impact of K_p on $f'(\eta)$, $g'(\eta)$

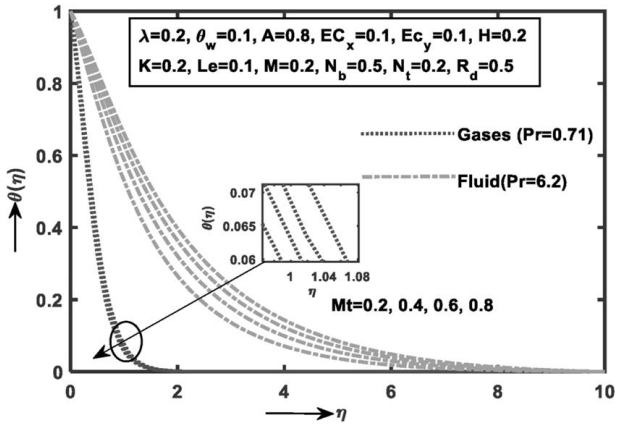

Fig. 4 Impact of *Mt* on $\theta(\eta)$

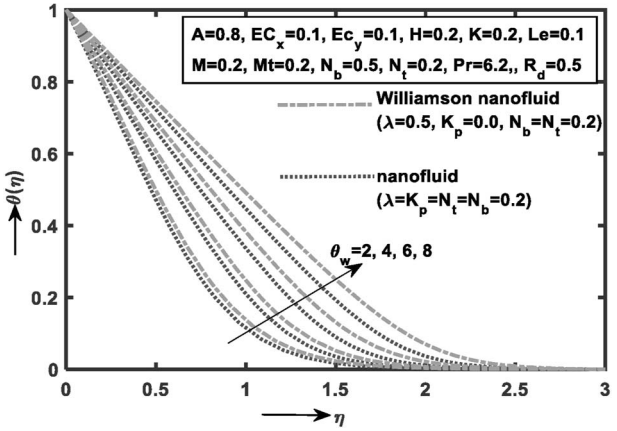

Fig. 5 Impact of θ_w on $\theta(\eta)$

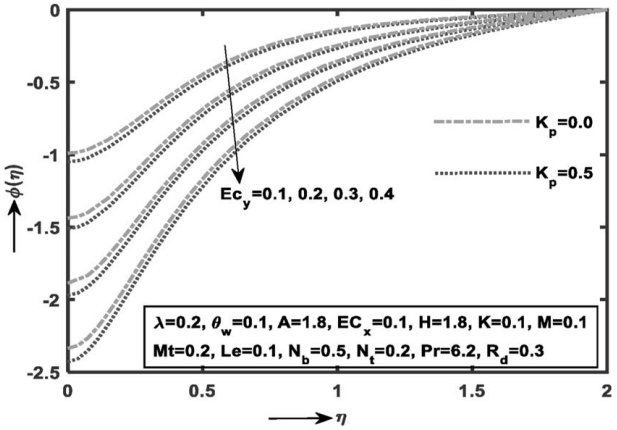

Fig. 6 Impact of Ec_y on $\phi(\eta)$

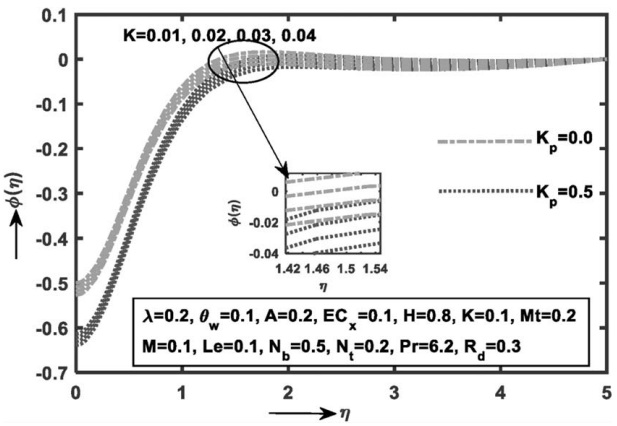

Fig. 7 Impact of *K* on $\phi(\eta)$

fluid case and nanofluid case are discussed, and the Prandtl number ($\Pr = 6.2$) value of water is taken in this study.

The variant of the non-Newtonian first Rivlin–Erickson tensor [15] of the fluid declines through "Williamson parameter" (λ) on axial and transverse velocity ($f'(\eta)$) and ($g'(\eta)$) is shown in Fig. 2. It is demonstrated that the velocity in both axes is diminished with high numerical values of λ. Physically, Williamson fluid is inversely proportional to kinematic viscosity. Due to this, the viscosity is control to velocity of Williamson fluid flow at surface.

The most significant effect K_p (porous parameter) on velocity in x- and y-directions of non-Newtonian nanofluid flow is shown in Fig. 3. The velocity should be diminished along x and y directions for higher values of K_p. Physically, when the motion of non-Newtonian fluid the Darcy resistance existing by porous medium k_p^* and choosing growth values of K_p correspond to strong resistance flow. Due to this, the fluid velocities are reduced for motion of the porosity surface.

Figure 4 shows the *Mt* (melting parameter) for fluid ($\Pr = 6.2$) and gas ($\Pr = 0.71$) cases on $\theta(\eta)$ in Williamson nanofluid motion. The melting heat transfer diminishes with distinct high values of *Mt*. It is clear that the convergence of the temperature function is monotonically decreasing with high significance for $\Pr = 6.2$ when compared with gases $\Pr = 0.71$. Physically, the melting parameter is inversely proportional to latent heat and heat

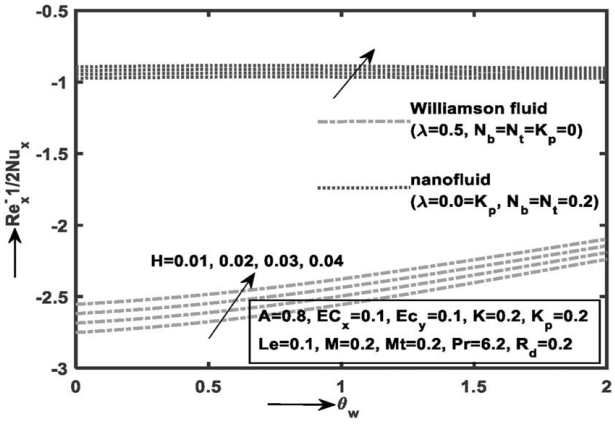

Fig. 8 Impact of H on $\mathrm{Re}_x^{-1/2}\mathrm{Nu}_x$

capacity of the solid surface. Due to this, the extra heat is transported from fluid heat toward a solid surface which leads to low convective flow.

The ($\theta_w = T_f/T_\infty$) (temperature ratio parameter) for the cases of Williamson nanofluid ($K_p = 0$, $N_t = N_b = 0.2$ $\lambda = 0.5$) and nanofluid ($K_p = \lambda = 0$, $N_t = N_b = 0.2$) on $\theta(\eta)$ is as shown in Fig. 5. It is noticed that the temperature distribution is convergent and monotonically increases with large values of θ_w (T_f/T_∞). The temperature function is monotonically converging at surface ($\eta = 1.5$) (not exact value) for Williamson nanofluid ($K_p = 0$, $N_t = N_b = 0.2$ $\lambda = 0.5$) and nanofluid ($K_p = \lambda = 0$, $N_t = N_b = 0.2$). It is concluded that there is high significant case of nanofluid flow when compared to the Williamson nanofluid case. Physically, the temperature ratio parameter is the interaction between fluid temperature toward surface and ambient temperature flow toward infinite surface. This means that the temperature ratio parameter depends strongly on surface temperature of the fluid.

The variation of viscous dissipation and Joule heating effects in non-Newtonian fluid motion in the presence ($K_p = 0.5$) and absence ($K_p = 0$) of porous medium on concentration function along the y-direction with high values of Ec_y (Eckert number) is shown in Fig. 6. It is demonstrated that the concentration of viscous dissipation and Joule heating influence amplify along the y-direction with high numerical values of Ec_y. Finally, there is high significant influence in the absence ($K_p = 0$) of a porous medium when comparing with the presence ($K_p = 0.5$) of the porous medium in non-Newtonian fluid motion.

The variation K (chemical reaction) influence in non-Newtonian fluid motion in the presence ($K_p = 0.5$) and absence ($K_p = 0$) of porous medium on the concentration function along stretching surface with high values of K is shown in Fig. 7. It is demonstrated that the concentration function reduces with higher values of K. Finally, in both the physical parameters there is high significant effects in the absence of porous medium ($K_p = 0$) when comparing in the presence of the porous medium ($K_p = 0.5$) in non-Newtonian fluid motion on the surface.

Figure 8 shows the variation of $\mathrm{Re}_x^{-1/2}Nu_x$ (heat transfer rate) with various choosing values of H (heat generation) via θ_w for the cases of Williamson fluid ($K_p = 0$, $N_t = N_b = 0$ $\lambda = 0.2$) and nanofluid ($K_p = 0$, $N_t = N_b = 0.2$ $\lambda = 0$). It is demonstrated that the rate of heat transport increases with higher values of H and Ec_x. Finally, heat transfer significantly increased in nanofluid motion which is more than the Williamson fluid motion on a stretching surface.

Conclusions

This article is related to the influence of nonlinear thermal radiative and heat generation on 3D magnetohydrodynamic Williamson nanofluid flow with chemical reaction over a linear stretching surface in the presence of the melting condition. It is analyzed with the numerical technique with the fourth-order Runge–Kutta–Fehlberg algorithm.The main outcomes in the present mathematical model is as follows:

- The Williamson nanofluid velocity motion in a porous medium along x- and y-directions slowly converges to zero at stretching surface ($\eta \to 0$) with increased values of K_p, M, and λ.
- The stretching ratio parameter increases in Williamson nanofluid velocity motion along the x-direction and decreases to zero at a porous surface ($\eta \to 0$) while a reverse trend occurs in the y-direction.
- The melting influence decrease is more convergent variation on $\theta(\eta)$ in the case of fluid value ($\mathrm{Pr} = 0.71$) when compared to gas value ($\mathrm{Pr} = 6.2$) with large values of Mt.
- The concentration reduction has more variation in the absence of porous medium ($K_p = 0$) when compared to gas value ($K_p = 0.2$) with large values of Ec_y and K.
- Overall, the heat transfer rate generation in Williamson nanofluid is more affected than the nanofluid at the same time pure fluid is more than the Williamson nanofluid and also regular fluid is more affected than the nanofluid.

Acknowledgment

The authors are grateful to the reviewers for their suggestions that extensively improved our paper.

Conflict of Interest

All procedures performed for studies involving human participants were in accordance with the ethical standards stated in the 1964 Declaration of Helsinki and its later amendments or comparable ethical standards? Informed consent was obtained from all participants. Documentation will be provided upon request. Informed consent was obtained for all individuals. This article does not include any research in which animal participants were involved.

Data Availability Statement

The authors attest that all data for this study are included in the paper.

Nomenclature

f = dimensionless stream function
k = thermal conductivity
p = hydrostatic pressure
t = time
A = stretching ratio parameter = b/a
C = volume fraction of nanoparticle
I = identity tensor
K = chemical reaction parameter = K_m/a
M = magnetic field parameter = $\sigma^* B_0^2/a\rho$
S = extra tensor
T = temperature
V = velocity field
c_p = specific heat (J kg K)
c_s = surface heat capacity
q_r = radiative heat flux ($W\,m^{-2}$)
A_1 = first Rivlin–Erickson tensor
B_0 = magnetic field strength
C_f = skin-friction coefficient
C_∞ = uniform ambient concentration
D_B = Brownian diffusion
D_T = thermophoresis diffusion ($m^2\,s^{-1}$)
K_m = chemical reaction
K_p = porous parameter = υ/k_p^*

N_b = Brownian motion coefficient = $\zeta D_B(C_w - C_\infty)/\alpha$
N_t = thermophoresis parameter = $\zeta D_T(T_w - T_\infty)/T_\infty\alpha$
Q_0 = heat generation
R_d = radiation parameter = $16\sigma^* T_\infty^2/3kk^*$
T_f = fluid temperature
T_m = melting temperature
T_s = surface temperature
T_w = temperature at the wall
T_∞ = ambient fluid temperature
U_w = stretching velocity along the y-direction
V_w = stretching velocity along the x-direction
b^* = constant
f' = dimensionless velocity
k^* = mean absorption coefficient
Ec_x = Eckert number in the direction of $x = u_w^2/(c_p)_f(T_w - T_\infty)$
Ec_y = Eckert number in the direction of $y = v_w^2/(c_p)_f(T_w - T_\infty)$
Re_x = Reynolds number
k_p^* = porosity
Le = Lewis number = α_m/D_B
Mt = melting parameter $(T_f - T_\infty)/(\beta + c_s(T_m - T_s))$
Pr = Prandtl number = (υ/α_m)
a, b = constants
u, v, w = velocity components
(x, y, z) = Cartesian coordinate's
d/dt = material derivative
∇ = operator

Greek Symbols

β = latent heat of the fluid
Γ = positive time-dependent material constant
ζ = ratio of the heat capacity and heat capacity nanoparticle of the fluid $(\rho c)_p/(\rho c)_f$
η = similarity variable
θ = dimensionless temperature
λ = Williamson parameter $\Gamma x\sqrt{2a^3/\upsilon}$
μ = dynamic viscosity
π = second invariant strain tensor
ρ = density
σ = Boltzmann constant (W m^{-2} K^{-4})
τ = Cauchy tensor
υ = kinematic viscosity
ϕ = dimensionless concentration
α_m = thermal diffusion = k/ρ
$\dot{\gamma}$ = shear rate
μ_0 = limiting viscosity at zero shear rate
μ_∞ = limiting viscosity at infinity shear rate
ρ_f = fluid density
$(\rho c)_f$ = heat capacity of the fluid
$(\rho c)_p$ = heat capacity of the nanoparticle to the fluid
σ^* = electrical conductivity ($\mathrm{m}^2 s^{-1}$)

Subscript

∞ = condition at freestream

References

[1] Williamson, R. V., 1929, "The Flow of Pseudoplastic Materials," Ind. Eng. Chem. Res., **21**(11), pp. 1108–1111.

[2] Bilal, S., Rehman, K. U., and Malik, M. Y., 2017, "Numerical Investigation of Thermally Stratified Williamson Fluid Flow Over a Cylindrical Surface Via Keller Box Method," Results Phys., **7**, pp. 690–696.

[3] Williamson, R. V., 1988, "The Flow of Pseudoplastic Materials," Ind. Eng. Chem. Res., **21**, pp. 108–111.

[4] Malik, M. Y., Bilal, S., Salahuddin, T., and Rehman, K. U., 2017, "Three-Dimensional Williamson Fluid Flow Over a Linear Stretching Surface," Math. Sci. Lett., **6**(1), pp. 53–61.

[5] Amanulla, C. H., Nagendra, N., Subba Rao, A., Anwar Bég, O., and Kadir, A., 2017, "Numerical Exploration of Thermal Radiation and Biot Number Effects on the Flow of a Non-Newtonian MHD Williamson Fluid Over a Vertical Convective Surface," Heat Transfer Asian Res., **47**(2), pp. 1–19.

[6] Moatimid, G. M., and Hassan, M. A., 2017, "Convection Instability of Non-Newtonian Walter's Nanofluid Along a Vertical Layer," J. Egypt. Math. Soc., **25**(2), pp. 220–229.

[7] Khan, W., Gul, T., Idrees, M., Islam, S., Khan, I., and Dennis, L. C. C., 2016, "Thin Film Williamson Nanofluid Flow With Varying Viscosity and Thermal Conductivity on a Time-Dependent Stretching Sheet," Appl. Sci., **6**(334), pp. 1–23.

[8] Parmar, A., 2017, "Unsteady Convective Boundary Layer Flow for MHD Williamson Fluid Over an Inclined Porous Stretching Sheet With Non-Linear Radiation and Heat Source," Int. J. Appl. Comput. Math., **3**(S1), pp. S859–S881.

[9] Bhatti, M. M., and Rashidi, M. M., 2016, "Effects of Thermo-Diffusion and Thermal Radiation on Williamson Nanofluid Over a Porous Shrinking/Stretching Sheet," J. Mol. Liq., **221**, pp. 567–573.

[10] Hayat, T., Ullah, I., Alsaedi, A., and Asghar, S., 2018, "Flow of Magneto Williamson Nanoliquid Towards Stretching Sheet With Variable Thickness and Double Stratification," Radiat. Phys. Chem., **152**, pp. 151–157.

[11] Satya Narayan, P. V., Tarakaramu, N., Makinde, O. D., Venkateswarlu, B., and Sarojamma, G., 2018, "MHD Stagnation Point Flow of Viscoelastic Nanofluid Past a Convectively Heated Stretching Surface," Defect Diffus. Forum, **387**, pp. 106–120.

[12] Ganesh Kumar, K., Rudraswamy, N. G., Gireesha, B. J., and Manjunatha, S., 2017, "Non-linear Thermal Radiation Effect on Williamson Fluid With Particle-Liquid Suspension Past a Stretching Surface," Results Phys., **7**, pp. 3196–3202.

[13] Satya Narayana, P. V., 2017, "Lie Group Analysis for the Flow and Heat Transfer of a Nanofluid Over a Stretching Sheet With Viscous Dissipation," J. Nanofluids, **6**, pp. 181–1187.

[14] Bilal, M., Sagheer, M., and Hussain, S., 2017, "Three-Dimensional MHD Upper-Convected Maxwell Nanofluid Flow With Nonlinear Radiative Heat Flux," Alexandria Eng. J., **57**(3), pp. 1917–1925.

[15] Shawky, H. M., Eldabe, N. T. M., Kamel, K. A., and Abd-Aziz, E. A., 2019, "MHD Flow With Heat and Mass Transfer of Williamson Nanofluid Over Stretching Sheet Through Porous Medium," Microsyst. Technol., **25**(4), pp. 1155–1169.

[16] Satya Narayana, P. V., Tarakaramu, N., Akshit, S. M., and Ghori, J. P., 2017, "MHD Flow and Heat Transfer of an Eyring–Powell Fluid Over a Linear Stretching Sheet With Viscous Dissipation—A Numerical Study," Front. Heat Mass Transfer, **9**(1), pp. 1–5.

[17] Venkateswarlu, B., Satya Narayana, P. V., and Tarakaramu, N., 2018, "Melting and Viscous Dissipation Effects on MHD Flow Over a Moving Surface With Constant Heat Source," Trans. A. Razmadze Math. Inst., **172**(3), pp. 619–630.

[18] Hajabdollahi, F., Premnath, K. N., and Malepati, S., 2018, "Effects of the Magnetic Field on Direct Contact Melting Transport Processes During Rotation," Appl. Math. Model., **61**, pp. 421–442.

[19] Huang, B., Zhai, Y., Liu, S., and Mao, X., 2018, "Microstructure Anisotropy and Its Effect on Mechanical Properties of Reduced Activation Ferritic/Martensitic Steel Fabricated by Selective Laser Melting," J. Nucl. Mater., **500**, pp. 33–41.

[20] Hayat, T., Saif, R. S., Ellahi, R., Muhammad, T., and Alsaedi, A., 2018, "Simultaneous Effects of Melting Heat and Internal Heat Generation in Stagnation Point Flow of Jeffrey Fluid Towards a Nonlinear Stretching Surface With Variable Thickness," Int. J. Therm. Sci., **132**, pp. 344–354.

[21] Cao, X., Yuan, Y., Xiang, B., and Haghighat, F., 2018, "Effect of Natural Convection on Melting Performance of Eccentric Horizontal Shell and Tube Latent Heat Storage Unit," Sustain. Cities Soc., **38**, pp. 571–581.

[22] Sheikholeslami, M., and Rokni, H. B., 2017, "Effect of Melting Heat Transfer on Nanofluid Flow in Existence of Magnetic Field Considering Buongiorno Model," Chin. J. Phys., **55**(4), pp. 1115–1126.

[23] Fauzi, N. F., Merkin, J. H., Ahmad, S., and Pop, I., 2017, "The Mixed Convection Boundary Layer on a Vertical Melting Front in a Non-Darcian Porous Medium," Transp. Porous Media, **116**(2), pp. 521–532.

[24] Sufiiarov, V. S., Popovich, A. A., Borisov, E. V., Polozov, I. A., Masaylo, D. V., and Orlov, A. V., 2017, "The Effect of Layer Thickness at Selective Laser Melting, Global Congress Manufacturing Management," Procedia Eng., **174**, pp. 126–134.

[25] Sheikholeslami1, M., Nimafar, M., and Ganji, D. D., 2017, "Analytical Approach for the Effect of Melting Heat Transfer on Nanofluid Heat Transfer," Eur. Phys. J. Plus., **132**(385), pp. 1–12.

[26] Khan, M. I., Waqas, M., Hayat, T., Khan, M. I., and Alsaedi, A., 2018, "Melting Heat Transfer in Stagnation Point of Carreau Fluid With Nonlinear Thermal Radiation and Heat Source," J. Braz. Soc. Mech. Sci. Eng., **40**(270), pp. 1–8.

[27] Ramzan, M., Bilal, M., and Chung, J. D., 2017, "MHD Stagnation Point Cattaneo–Christov Heat Flux in Williamson Fluid Flow With Homogeneous–Heterogeneous Reactions and Convective Boundary Condition—A Numerical Approach," J. Mol. Liq., **225**, pp. 856–862.

[28] Krishnamurthy, M. R., Prasannakumara, B. C., Gireesha, B. J., and Rama Subba Reddy, G., 2016, "Effect of Chemical Reaction on MHD Boundary Layer Flow and Melting Heat Transfer of Williamson Nanofluid in Porous Medium," Eng. Sci. Technol. Int. J., **19**, pp. 53–61.

[29] Ramzan, M., Bilal, M., and Chung, J. D., 2017, "Radiative Williamson Nanofluid Flow Over a Convectively Heated Riga Plate With Chemical Reaction—A Numerical Approach," Chin. J. Phys., **55**(4), pp. 1663–1673.

[30] Hayat, T., Muhammad, K., Alsaedi, A., and Asghar, S., 2018, "Numerical Study for Melting Heat Transfer and Homogeneous–Heterogeneous Reactions in Flow Involving Carbon Nanotubes," Results Phys., **8**, pp. 415–421.

[31] Tarakaramu, N., and Satya Narayan, P. V., 2017, "Unsteady MHD Nanofluid Flow Over a Stretching Sheet With Chemical Reaction," IOP Conf. Ser.: Mater. Sci. Eng., **263**, pp. 1–8.
[32] Raju, D., 2017, "Heat and Mass Transfer to Unsteady MHD Viscoelastic Slip Flow Through a Porous Medium With Chemical Reaction," Int. J. Future Revolution Comput. Sci. Commun. Eng., **3**(11), pp. 1–10.
[33] Jena, S., Mishra, S. R., and Dash, G. C., 2017, "Chemical Reaction Effect on MHD Jeffery Fluid Flow Over a Stretching Sheet Through Porous Media With Heat Generation/Absorption," Int. J. Appl. Comput. Math., **3**, pp. 1–14.
[34] Ramamohan Reddy, L., Raju, M. C., Raju, G. S. S., and Ibrahim, S. M., 2017, "Chemical Reaction and Thermal Radiation Effects on MHD Micropolar Fluid Past a Stretching Sheet Embedded in a Non-Darcian Porous Medium," J. Comput. Appl. Res. Mech. Eng., **6**(2), pp. 27–46.
[35] Khan, M. I., Waqas, M., Hayat, T., and Alsaedi, A., 2017, "A Comparative Study of Casson Fluid With Homogeneous–Heterogeneous Reactions," J. Colloid Interface Sci., **498**, pp. 85–90.
[36] Hayat, T., Khan, M. I., Waqas, M., Alsaedi, A., and Yasmeen, T., 2017, "Diffusion of Chemically Reactive Species in Third Grade Fluid Flow Over an Exponentially Stretching Sheet Considering Magnetic Field Effects," Chin. J. Chem. Eng., **25**(3), pp. 257–263.
[37] Bilal Ashraf, M., Alsaedi, A., Hayat, T., and Shehzad, S. A., 2017, "Convective Heat and Mass Transfer in Three-Dimensional Mixed Convection Flow of Viscoelastic Fluid in Presence of Chemical Reaction and Heat Source/Sink," Comput. Math. Math. Phys., **57**(6), pp. 1066–1079.
[38] Ganesh Kumar, K., Rudraswamy, N. G., Gireesha, B. J., and Krishnamurthy, M. R., 2017, "Influence of Nonlinear Thermal Radiation and Viscous Dissipation on Three-Dimensional Flow of Jeffrey Nano Fluid Over a Stretching Sheet in the Presence of Joule Heating," Nonlinear Eng., **6**(3), pp. 1–13.
[39] Khan, M. I., Alsaedi, A., Shehzad, S. A., and Hayat, T., 2017, "Hydromagnetic Nonlinear Thermally Radiative Nanoliquid Flow With Newtonian Heat and Mass Conditions," Results Phys., **7**, pp. 2255–2260.
[40] Ganesh Kumar, K., Gireesha, B. J., Manjunatha, S., and Rudraswamy, N. G., 2017, "Effect of Nonlinear Thermal Radiation on Double-Diffusive Mixed Convection Boundary Layer Flow of Viscoelastic Nanofluid Over a Stretching Sheet," Int. J. Mech. Mater. Eng., **12**(18), pp. 1–18.
[41] Khan, M., Irfan, M., Khan, W. A., and Ahmad, L., 2017, "Modeling and Simulation for 3D Magneto Eyring–Powell Nanomaterial Subject to Nonlinear Thermal Radiation and Convective Heating," Results Phys., **7**, pp. 1899–1906.
[42] Hayat, T., Qayyum, S., Alsaedi, A., and Shafiq, A., 2016, "Inclined Magnetic Field and Heat Source/Sink Aspects in Flow of Nanofluid With Nonlinear Thermal Radiation," Int. J. Heat Mass Transfer, **103**, pp. 99–107.
[43] López, A., Ibáñez, G., Pantoja, J., Moreira, J., and Lastres, O., 2017, "Entropy Generation Analysis of MHD Nanofluid Flow in a Porous Vertical Microchannel With Nonlinear Thermal Radiation, Slip Flow and Convective-Radiative Boundary Conditions," Int. J. Heat Mass Transfer, **107**, pp. 982–994.
[44] Tarakaramu, N., Satya Narayana, P. V., Sivajothi, R., Bhagya Lakshmi, K., Harish Babu, D., and Venkateswarlu, B., 2022, "Three-Dimensional Non-Newtonian Couple Stress Fluid Flow Over a Permeable Stretching Surface With Nonlinear Thermal Radiation and Heat Source Effects," Heat Transfer, **51**(6), pp. 5348–5367.